magnetochemistry

MDPI

Article

Magnetism and Exchange Bias Properties in Ba_2ScRuO_6

Prachi Mohanty [1,†], Sourav Marik [2,*] and Ravi Prakash Singh [1,*]

[1] Indian Institute of Science Education and Research Bhopal, Bhopal 462066, Madhya Pradesh, India
[2] School of Physics and Materials Science, Thapar Institute of Engineering and Technology, Patiala 147004, Punjab, India
* Correspondence: soumarik@thapar.edu (S.M.); rpsingh@iiserb.ac.in (R.P.S.)
† Current address: Department of Physics, Odisha University of Technology and Research, Bhubaneswar 751003, Odisha, India.

Abstract: This paper presents structural, detailed magnetic, and exchange bias studies in polycrystalline Ba_2ScRuO_6 synthesized at ambient pressure. In contrast to its strontium analogue, this material crystallizes in a 6L hexagonal structure with space group $P\bar{3}m1$. The Rietveld refinement using the room-temperature powder XRD pattern suggests a Ru-Sc disorder in the structure. The temperature variation of the DC electrical resistivity highlights a semiconducting behavior with the electron conduction corresponding to Mott's 3D variable range hopping (VRH) model. The detailed magnetization measurements show that Ba_2ScRuO_6 develops antiferromagnetic ordering at $T_N \approx 9$ K. Interestingly, below 9 K (T_N), the field-cooled magnetic field variation (FC) of the magnetization curves highlights an exchange bias effect in the sample. The exchange bias field reaches a maximum value of 1.24 kOe at 2 K. The exchange bias effect below the magnetic ordering temperature can be attributed to the inhomogeneous magnetic correlations due to the disorder in the structure. Remarkably, the appearance of a large exchange bias field in Ba_2ScRuO_6 indicates that inhomogeneous hexagonal double perovskites are a promising class to explore new materials having potential applications in spintronics.

Keywords: ruthenates; exchange bias; double perovskites

Citation: Mohanty, P.; Marik, S.; Singh, R.P. Magnetism and Exchange Bias Properties in Ba_2ScRuO_6. *Magnetochemistry* **2023**, *9*, 144. https://doi.org/10.3390/magnetochemistry9060144

Academic Editor: Hiromasa Goto

Received: 24 April 2023
Revised: 17 May 2023
Accepted: 22 May 2023
Published: 29 May 2023

1. Introduction

Double perovskites (DPs), discovered in 1889, with a general formula $A_2BB'O_6$ (A = Alkaline metals, B and B′ = transition metals) have attracted intense research attention as these materials are known to host intriguing magnetic and magneto-transport properties having potential applications in spintronics [1–6]. In an ideal DP structure, the two transition metal sites (B and B′) form interpenetrating face-centered cubic (FCC) sublattices. As a structural feature of DPs, the intra- and inter-sublattice superexchange couplings and their interactions determine the complex magnetic properties of the system [7–10]. However, double perovskites with a magnetic ion at the B′ site (B = nonmagnetic) attracted recent interest due to their potential to design an enhanced magnetic frustration and exchange bias effect [11,12].

Among double perovskites, the ruthenium-based DP with composition A_2BRuO_6 (B = smaller metals) is an important family of DPs due to its rich structural variation and diverse range of exotic magnetic behavior [11–26]. The structure has two nonequivalent crystallographic sites for Ru- and B-type cations. This arrangement is similar to a geometrically frustrated edge-shared tetrahedra network; therefore, the antiferromagnetic (AF) correlations are frustrated. Nevertheless, several Ru^{5+} DPs show exotic magnetic behavior and long-range antiferromagnetic ordering despite a high magnetic frustration. For instance, Ba_2YRuO_6 (cubic) [11] shows a very high Curie-Weiss temperature (−522 K); however, a long-range magnetic ordering is observed at 37 K and Sr_2YRuO_6 shows magnetization reversal and exchange bias-like properties [19,22,27]. Monoclinic La_2LiRuO_6

and La_2NaRuO_6 also show long-range magnetic ordering despite high magnetic frustrations [28,29]. In addition to the interesting half-filled configuration of Ru^{5+} (t_{2g}^3, S = 3/2) cations, the role of spin-orbit coupling (SOC) is also crucial in determining the magnetic and physical properties of materials containing 4d (and 5d) [20]. Furthermore, the presence of nonmagnetic B cations and their distribution in the structure can affect the strength of the magnetic correlations. Recently, structurally inhomogeneous double perovskite systems became a topic of immense research due to their potential to show the technologically important exchange bias effect. For instance, the inverse exchange bias effect is observed in (cationic) disordered Gd_2CoRuO_6 [30]. The antisite disorder in $LaSrCoFeO_6$ shows a large exchange bias effect with an exchange bias field of 1.2 kOe at 5 K [31]. The antisite disorder in Sm-doped La_2NiMnO_6 triggers an exchange bias and a spin glass effect [32].

Recently, Kayser et al. [33] highlighted a new Ru-Sc-based double perovskite. Their study showed that the ambient pressure synthesized Ba_2ScRuO_6 can be stabilized in a 6L hexagonal structure. Interestingly, a disorder of Ru-Sc was observed in the structure. The inhomogeneous distribution of magnetic and nonmagnetic cations in different crystallographic sites in a 6L-type hexagonal structure can cause the emergence of exotic magnetic behavior, such as frustrated magnetism and the exchange bias effect in this compound. Further, the detailed magnetic properties (including the exchange bias effect) have not been explored as yet. Therefore, we explored the detailed magnetic and exchange bias properties in Ba_2ScRuO_6. Here, we report the detailed magnetic properties and a large exchange bias effect in this ruthenium DP compound. Detailed studies on the cooling field and the influence of temperature on the exchange bias and training effects are presented here.

2. Experimental Section

A standard solid-state reaction method was used to synthesize the polycrystalline Ba_2ScRuO_6 material. Stoichiometric amounts of $BaCO_3$ (99.95%, Sigma-Aldrich, St. Louis, MO, USA), Sc_2O_3 (99.99%, Sigma-Aldrich), and RuO_2 (99.9%, Sigma-Aldrich) were homogenized using a mortar and pestel. The sample was first heat treated at 960 °C and then at 1400 °C for 72 h in an air atmosphere. Each step involved several intermediate grinding and pelleting. Powder X-ray diffraction (XRD) patterns were collected at room temperature (RT) using a PANalytical X'pert PRO diffractometer (Cu Kα-radiation, λ = 1.5406). Phase purity and structural analysis were performed by Rietveld analysis using the RT-XRD patterns (using Full Prof suite software (for Windows, Linux and macOS) https://www.ill.eu/sites/fullprof/ accessed on 21 May 2023). Electrical resistivity (ρ) data as a function of temperature were collected in the absence of a magnetic field using a Physical Property Measurement System (PPMS, Quantum Design (San Diego, CA, USA)). The temperature-dependent resistivity measurement was carried out using the DC four-probe method. Magnetization measurements as a function of temperature and magnetic field were performed using a Quantum Design MPMS-3 magnetometer. We collected magnetization data in the temperature range of 1.9 K $<$ T $<$ 400 K. The magnetic field variations of the magnetization loops (M-H) were measured between $\pm$2.5 kOe.

3. Results and Discussion

The phase purity and crystal structure were determined using the room temperature (RT) X-ray diffraction pattern (XRD). The Rietveld refinement of the room-temperature X-ray diffraction pattern (Figure 1) highlights that Ba_2ScRuO_6 crystallizes in a hexagonal phase, space group (S.G.) $P\bar{3}m1$ with the Sc and Ru ordering in alternate (001) layers. The final results of the structural analysis (cell parameters and atomic positions) using the RT-XRD pattern are listed in Table 1. The lattice parameters obtained are a = b = 5.80946 (3) Åand c = 14.3028 (3) Åand are in good agreement with the previous report [33]. Four different crystallographic sites (Sc1 (1b, 0, 0, 0.5), Ru1 (2d, 0.33, 0.67, z), Sc2 (1a, 0, 0, 0) and Ru2 (2d, 0.33, 0.67, z)) are used to describe the positions of the Sc and Ru cations (in the crystal structure as shown in Figure 1b they are depicted as M1 (1b), M4 (2d), M3 (1a) and M4 (2d)). As suggested by Kayser et al. [33], in our refinement, a disorder of Ru-Sc is

considered in our refinement. The Ru-Sc disorder is observed at crystallographic sites of Sc2 (M3, 1a) and Ru2 (M4, 2d). However, the other two sites, M and M2, are entirely filled by Sc (M1, 1b) and Ru (M2, 2d) cations, respectively. The refinements of the occupancy of the Ba show full occupancy. The positions of the oxygen atoms in the structure are described using three different oxygen positions (Table 1). However, the occupancy of the oxygen positions was fixed during the refinement. A view of the crystal structure for Ba_2ScRuO_6 material is depicted in Figure 1b. The structure involves the face-sharing M_2O_9 dimeric units linked by a single corner sharing MO_6 octahedral units. Octahedra with Sc atoms in the center constitute sets of corner-shared MO_6 units. However, the Ru cations occupy the face-sharing positions and connect to the Sc-centered octahedra by corner-sharing. Furthermore, we estimated the crystallite size D = 46 nm using the Debye-Scherrer formula [$D = k\lambda/(\beta cos\theta)$, k = shape factor, considered as 0.9, λ = wavelength, β = full-width half maximum, and θ = Bragg angle] [34].

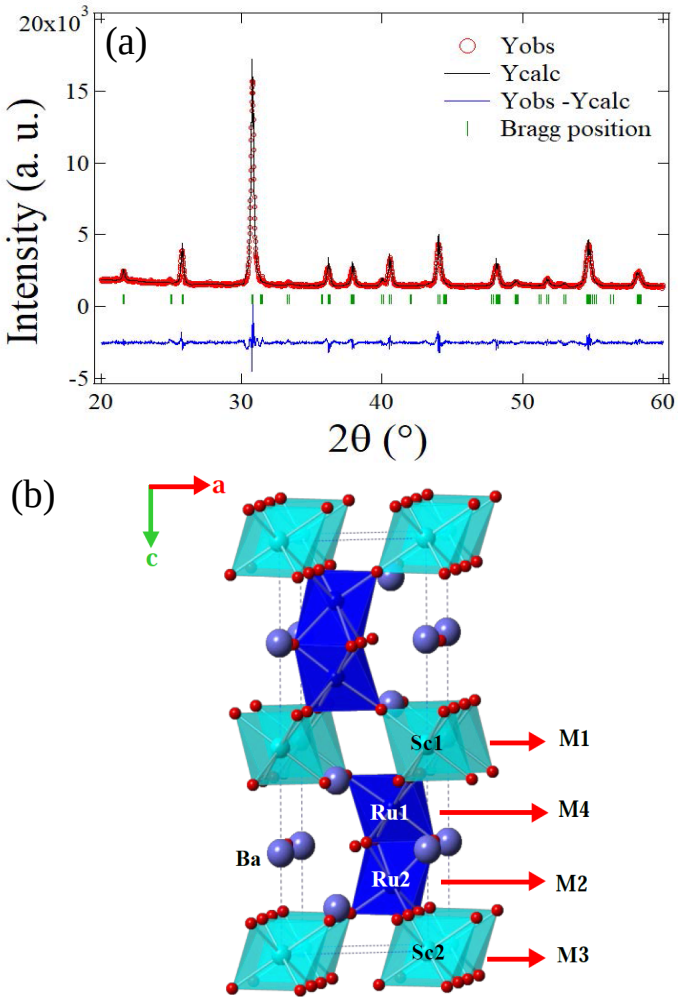

Figure 1. (**a**) Rietveld refinement plot of the X-ray powder diffraction pattern obtained at room temperature and (**b**) the hexagonal perovskite-type structure representation (space group $P\bar{3}m1$) for Ba_2ScRuO_6. The Ba atoms are shown as blue spheres. Oxygen atoms are highlighted as red spheres. The center of the polyhedra is occupied by Sc and Ru cations. Ru occupies mainly the M2 and M4 sites (face-shared). Scandium occupies the corner-shared M1 and M3 sites.

Table 1. Structural parameters for Ba_2ScRuO_6 at RT extracted from Rietveld refinement of the XRD powder diffraction data.

Atom	Wyck. Position	x	y	z
Ba1	2c	0	0	0.25
Ba2	2d	0.33	0.67	0.102
Ba3	2d	0.33	0.67	0.413
Sc1 (M1)	1b	0	0	0.5
Sc2 (M3)	1a	0	0	0
Ru1 (M2)	2d	0.33	0.67	0.661
Ru2 (M4)	2d	0.33	0.67	0.848
O1	6i	0.162	−0.162	0.299
O2	6i	0.820	−0.820	0.081
O3	6i	0.835	−0.835	0.415

Structure: Hexagonal, Space group: $P\bar{3}m1$; a (Å) = 5.80946(3), b (Å) = 5.80946(3), c (Å) = 14.3028(3); $\alpha = \beta = 90$ deg, $\gamma = 120$ deg, V_{cell}(Å^3) = 418.04.

To know about the DC electrical resistivity and its change as a function of temperature, we recorded the DC resistivity data in the absence of an external applied magnetic field using PPMS (Quantum Design). Figure 2 shows the plots of the logarithmic variation of ρ (electrical resistivity) as a function T^{-1} and $T^{-1/4}$ for Ba_2ScRuO_6 (in the bottom and top panels, respectively). The material displays an activated conductivity within the studied temperature zone, indicating a semiconducting-type behavior (inset in Figure 2). Previous studies on Ba_2ScRuO_6 highlight a semiconducting-type behavior with an activation energy of 0.207 eV [33]. As we decrease the temperature, the resistivity starts to increase. Below 150 K, it exceeds the measurement limit of the PPMS (Quantum Design). In the measurement limit (150–300 K), the slope of the ρ(T) plot is not constant but varies with temperature, suggesting Mott variable range hopping (VRH) type conductivity. In a disordered system, the low temperature conduction mechanism is usually described using the localized charge carrier known as the Mott-VRH model. According to Mott-VRH, $\sigma = \sigma_0 \exp[-(T_P/T)]^{1/(1+d)}$, [$\sigma$ = conductivity, d = dimensions, and T_P = characteristic temperature] [35]. Consistent with the 3D-VRH model is indicated by a roughly linear response of ln ρ (T) plotted on the $T^{-1/4}$ scale. However, ln ρ (T) vs. T^{-1} does not show linear behaviors. The linear response of ln ρ(T) plotted in $T^{-1/4}$ scale is analogous to the 3D-VRH transport model and is also realized for other disordered double perovskites, for instance, in Ca_2CoOsO_6 [36]. Therefore, the electron conduction corresponds to the Mott 3D-VRH model. Carriers are localized due to the disorder.

To understand the magnetic properties of this double perovskite compound, detailed magnetic measurements (magnetization as a function of temperature and magnetic field) were performed using a MPMS 3 magnetometer. Magnetic susceptibility measurements were performed after cooling the sample from RT to 2 K in a zero field-cooled (ZFC) and field-cooled (FC) mode and under several magnetic fields. The temperature dependence of the ZFC and FC susceptibility (χ- T) measured at an applied magnetic field H = 1 kOe for Ba_2ScRuO_6 is displayed in Figure 3a. The ZFC and FC curves are essentially indistinguishable up to ∼9 K. A slight divergence appears below 9 K, showing a magnetic transition. In the ZFC mode, the magnetization shows a pronounced maximum at ∼9 K, signalling a low temperature antiferromagnetic phase due to the magnetic ordering of the Ru^{5+} moments as Sc^{3+} cations are nonmagnetic. The irreversibility between the ZFC and FC curves may arise due to weak ferromagnetic components, which can possibly be attributed to the frustration between the ordered moments.

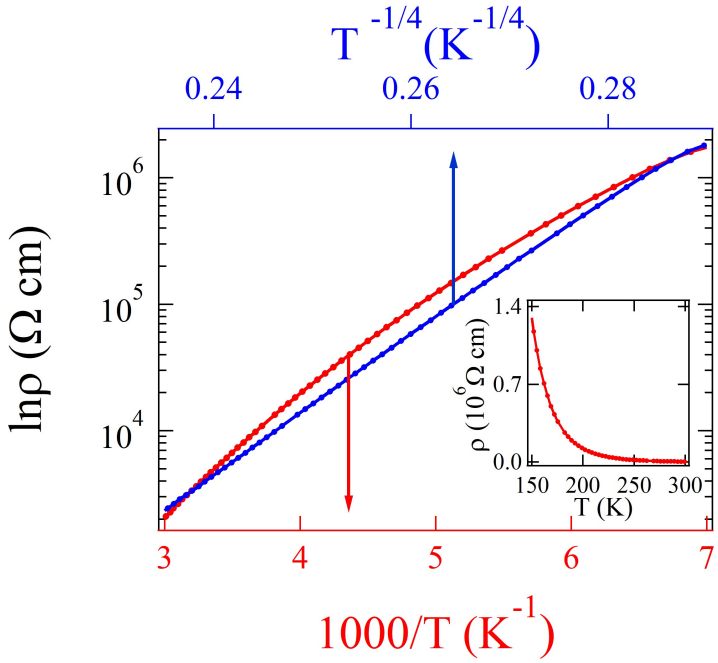

Figure 2. Electrical resistivity (ln ρ) as a function of T^{-1} and $T^{-1/4}$ (150 to 300 K) displayed on the bottom and top axes, respectively. The corresponding plot of resistivity vs temperature (ρ vs T) is shown in the inset.

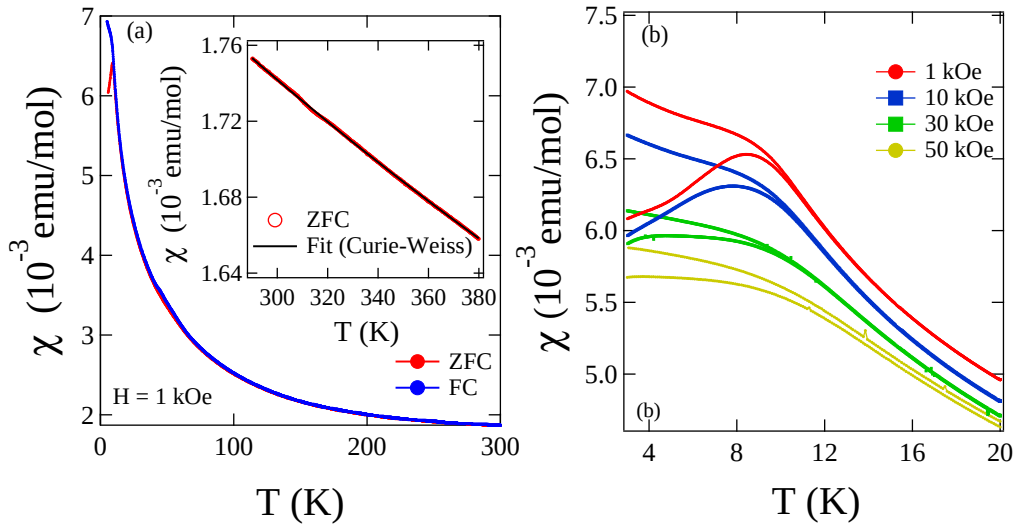

Figure 3. (**a**) Temperature variation of magnetic susceptibility (ZFC and FC, H = 1 kOe) for Ba_2ScRuO_6. (**b**) Temperature dependence of magnetic susceptibility curves (FC and ZFC) in different applied fields.

The ZFC and FC susceptibility plots after being normalized to the measuring field under several applied fields are illustrated in Figure 3b. The ordering temperature is shifted to lower temperatures for higher applied fields (>1 kOe). The modified Curie-Weiss fitting

$$\chi = \chi_0 + \frac{N\mu_B^2 p_{\text{eff}}^2}{3k_B(T-\theta_p)} \quad (1)$$

[where p_{eff} is the effective paramagnetic moment, θ_p is the paramagnetic Curie temperature, and χ_0 is the temperature independent term] in the paramagnetic region above 280 K is shown in the inset of Figure 3a. The black line represents the best fit (inset in Figure 3a) to the modified Curie-Weiss equation, which agrees with the experimental data in the high temperature interval. From the fitting between T = 290 K and 380 K, we obtained

the Curie constant C = 1.12 emu mol^{-1} K and the Weiss temperature θ = −694 K. The negative value indicates the strong antiferromagnetic correlations between the Ru^{5+} ions. Furthermore, the obtained Weiss temperature is very high and indicates the existence of the frustration of the magnetic moments at high temperatures. The effective magnetic moment (p_{eff}), obtained using C as 2.98 μ_B, slightly differs from the theoretical value for the Ru^{5+} ion (spin-only) with S = 3/2 μ_B (3.87 μ_B). However, the calculated value of p_{eff} is similar to those observed for other hexagonal perovskites containing Ru_2O_9 dimers, such as $Ba_3YRu_2O_9$ and $Ba_3LaRu_2O_9$ compounds [37]. This can be ascribed to the high spin frustration (f = 77).

The χ-T plots in the presence of several applied magnetic field are shown in Figure 3b. The susceptibility values show a decreasing trend with the increasing magnetic field near the magnetic ordering temperature. The susceptibility curves measured in low magnetic fields below T_N = 9 K show high irreversibilities between the ZFC and FC modes. However, increasing the applied magnetic field is found to suppress the irreversibility. The high irreversibility (ZFC and FC susceptibility) can also indicate a spin-glass-type transition. However, to obtain a deeper understanding of the magnetic state of Ba_2ScRuO_6, we performed AC susceptibility measurements at different frequencies (10 Hz and 1 kHz). Figure 4 shows the real part (χ'_{ac}) of our AC susceptibility measurements. The peak position in the AC susceptibility curves shows no frequency-dependent shift, confirming the absence of spin-glass-type behavior in Ba_2ScRuO_6. To further understand the magnetic behavior in detail, magnetic isotherms (M-H) were obtained between ±25 kOe at different temperatures (between 2 and 15 K) in zero field-cooling mode (Figure 5). A linear magnetization (AFM type) change with very small hysteresis behavior was observed. The small observed hysteresis could be due to frustration in the structure.

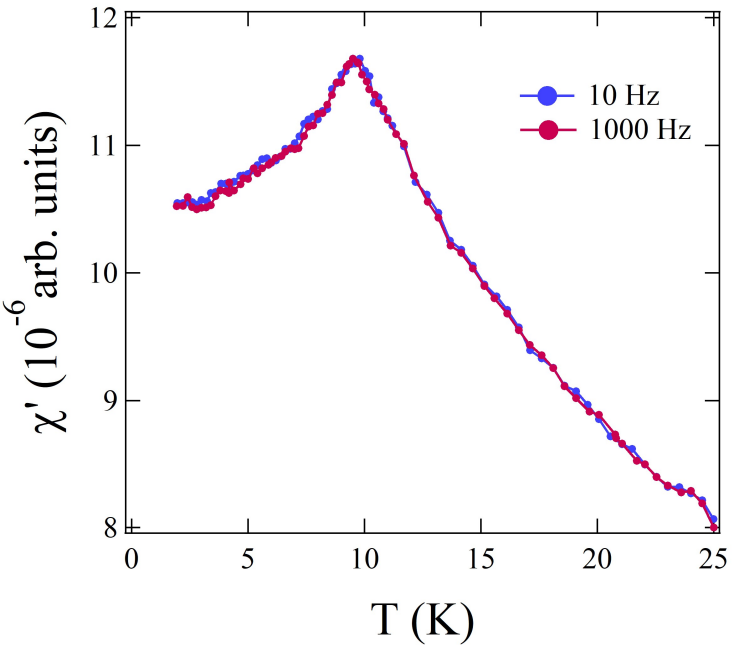

Figure 4. The temperature dependent real part (χ') of the AC susceptibility data for Ba_2ScRuO_6.

In recent times, there has been significant interest in exploring and understanding the effects of exchange bias (EB) in structurally inhomogeneous systems with various combinations of magnetic cations [30–32,38–41]. In the exchange bias effect, the field-cooled (FC) M-H loops show a shift along the magnetic field axis, and this is used in several technological applications, such as magnetic recording read heads [42], random access memories [43], and other spintronics devices [44,45]. To explore the EB behavior in the present sample, we measured M-H loops at selected temperatures in the field-cooling condition (H_{FC} = 20 kOe). The M-H loops were measured in the FC mode between ±25 kOe. For all

M-H measurements (ZFC and FC), the material was cooled from T > T_N to the measuring temperature (T_{meas}), and the *M-H* data were obtained in the field range ± 25 kOe when reached T_{meas}. The FC *M-H* curves measured at 2 K are shown in Figure 5. Interestingly, the field-cooled *M-H* loops shifted along the negative field axis. A representative result, as illustrated in Figure 6, highlights a shift of the center of the *M-H* curve along the negative magnetic field axis around 1.24 kOe. Being a classic signature of unidirectional anisotropy, the shift of the magnetization loop (*M-H*) reveals the surprising existence of the EB effect in Ba_2ScRuO_6. The offset of the *M-H* curve along the field axis can be denoted as the exchange bias field H_{EB} and the coercive field H_C, and can be extracted from the *M-H* loops [$H_C = (H_+ - H_-)/2$ and $H_{EB} = (H_+ + H_-)/2$, respectively. Here, H_+ and H_- are the coercivities in the ascending and descending branch of the *M-H* curve with a field axis].

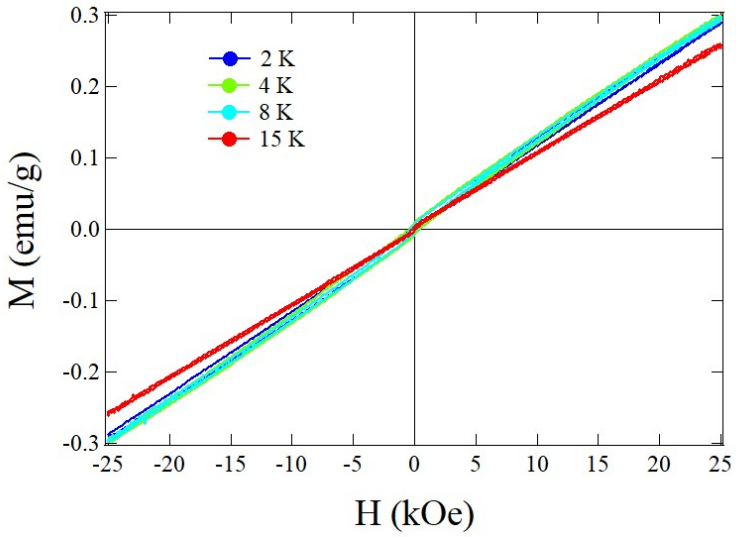

Figure 5. Zero field-cooled magnetization curves as a function of magnetic field (*M-H*) for Ba_2ScRuO_6 measured at several temperatures.

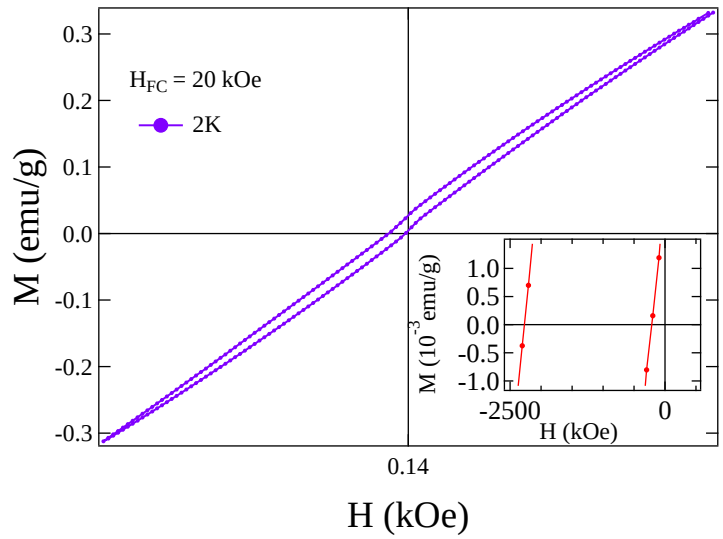

Figure 6. Field-cooled (H_{FC} = 20 kOe)) *M-H* loop for Ba_2ScRuO_6 measured at 2 K. The inset illustrates the enlarged central part of the FC *M-H* loop.

The choice of cooling field is extremely important in exchange bias measurements. To choose a suitable H_{FC} for Ba_2ScRuO_6, the *M-H* loops were obtained at 5 K while cooling the sample in different magnetic field ranging from 0.5 kOe to 40 kOe; this is depicted in Figure 7a. H_{EB} increases with the cooling field up to 10 kOe, and then it exhibits a

saturation tendency for H_{FC} above 10 kOe [see Figure 7b]. Therefore, we considered a cooling field of 20 kOe (more than 10 kOe) to study the EB effect in Ba_2ScRuO_6.

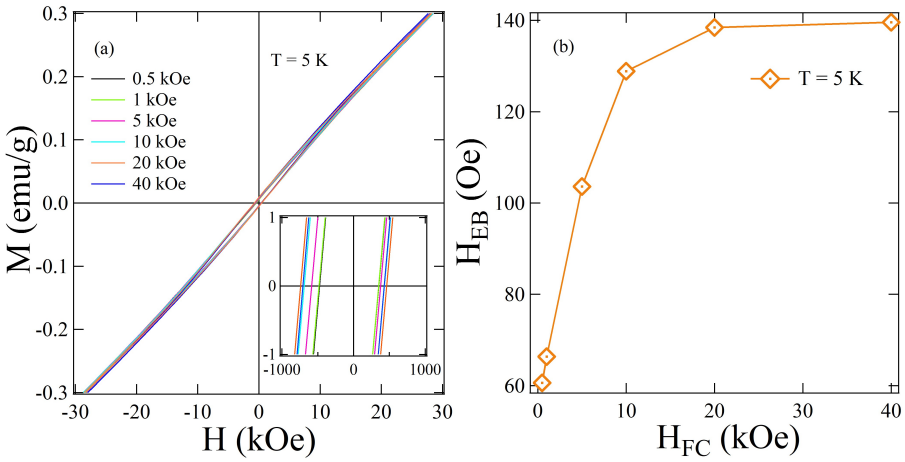

Figure 7. (**a**) *M-H* loops measured at T = 5 K with different H_{FC} values (0.5 kOe to 40 kOe). The inset highlights the central and enlarged part of the *M-H* loops. (**b**) Variation of H_{EB} with different values of H_{FC} (0.5 to 40 kOe).

It is important to know whether the exchange bias properties are associated with the long-range magnetic ordering in Ba_2ScRuO_6. Therefore, we measured several *M-H* curves at various fixed temperatures. The characteristic temperature-dependent trend of the exchange bias field and coercivity with the measuring temperature for Ba_2ScRuO_6 is summarized in Figure 8. A large value of the exchange bias field (H_{EB}) of 1.24 kOe is observed at 2 K. In comparison, the Ru-based disordered Gd_2CoRuO_6 shows a very small exchange bias field (≈160 Oe) below 5 K [30]. Double perovskite Sr_2YbRuO_6 shows a tunable exchange bias; however, the maximum exchange bias field is observed as ≈800 Oe at 2 K [46]. Very recently, in structurally disordered $Ba_3CoRu_2O_9$, a large exchange bias field of 3.48 kOe at 3 K is observed with a cooling field of 50 kOe [47]. However, a smooth decrease in the exchange bias field (H_{EB}) and the coercivity (H_c) is observed when increasing the temperature, eventually vanishing above T_N = 9 K. Therefore, the appearance of the exchange bias field and coercivity below the magnetic ordering temperature indicates its relation with the magnetic correlations in the structure. In addition, for the long-range AFM ordering (T_N = 9 K) the disorder in the Ru-Sc layers could create the magnetic frustration (Weiss temperature = −694 K, f = 77). The high magnetic frustration in the structure, therefore, can create e an exchange bias effect below T_N = 9 K.

The uncompensated spin configuration of the present system can relax from its equilibrium configuration in the presence of suitably applied magnetic fields. Therefore, the system is trained by increasing the number of successive hysteresis loops (*M-H*). In these connections, an important property generally highlighted in EB materials is the training effect. This can be described as reducing the exchange bias field H_{EB} as the M -H curve shrinks when cycling the material in several consecutive *M-H* loops. Figure 9a shows the enlarged version of the central portion of the representative magnetic loop recorded at 2 K in the negative field quadrant after the field cooled to 20 kOe. Here, a prominent training effect is observed. The H_{EB} as a function of the loop cycles (n) is shown in Figure 9b. The training effect is generally considered as a direct macroscopic fingerprint of the rearrangements of the spins toward equilibrium [see Figure 9] [48,49]. The training effect becomes prominent after the first magnetic field cycling due to the reconfiguration of the frozen spins. Reconfiguration in the spin structure results in a sharp decrease in H_{EB} after the first magnetic field cycle. Consequently, the change in H_{EB} after the second field cycling is moderate.

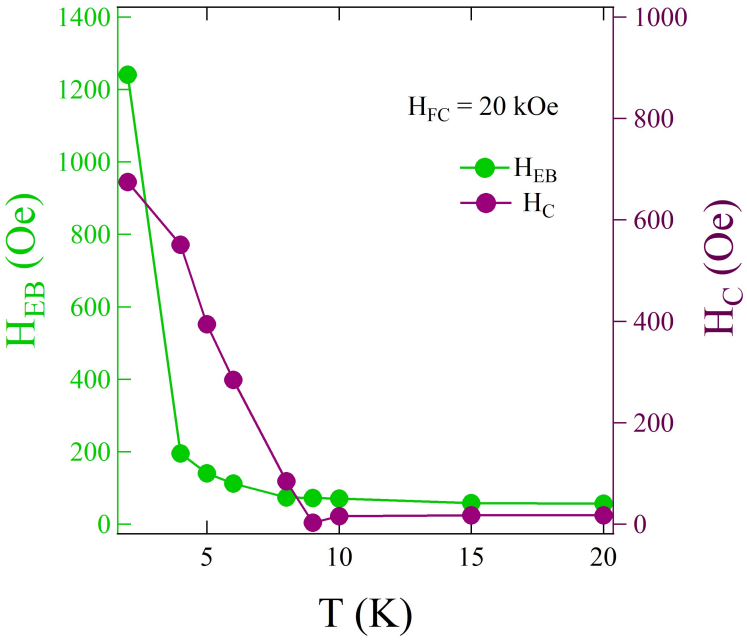

Figure 8. Left axis: Temperature dependent H_{EB} for Ba_2ScRuO_6. The H_{EB} values are obtained from the FC *M*-*H* curves measured at several temperatures. Right axis: Temperature dependent H_C obtained from the same *M*-*H* loops.

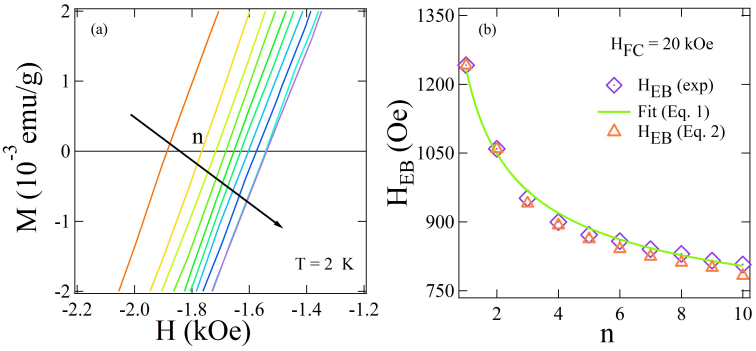

Figure 9. (**a**) The expanded view of the central part of the consecutive *M*-*H* loops. (**b**) The dependence of H_{EB} on the number of field cycles (n) (diamond markers) obtained from the consecutive *M*-*H* loops (training effect). The green line is the best fit to Equation (2) for $n > 1$. Data points in open triangles (orange) are generated using Equation (3).

The usual relationship between H_{EB} and n (for $n > 1$) that describes the relaxation of the EB effect is known to lead to a simple power law relationship [16]:

$$H_{EB}(n) - H_{E\infty} = k/\sqrt{n}. \quad (2)$$

Here, H_{EB} (n) = exchange bias field in the nth cycle, $H_{E\infty}$ = exchange field in the limit $n \to \infty$, and K = system-dependent constant. The best-fit results (dotted line) are shown in Figure 9b. The value of $H_{E\infty}$ obtained from the fitting is 606.24 Oe and this is the remnant $H_{E\infty}$ in the material.

Furthermore, an additional approach is required to explain the training effect since the power law as described in Equation (2) breaks down for $n = 1$. It was proposed in the framework of non-equilibrium thermodynamics, and it causes a relaxation toward equilibrium in the spin configuration of the interface magnetization (antiferromagnetic). In

fact, to better describe the exchange bias effect and its dependence on the number of field cycles (n), a recursive formula is considered [50]:

$$H_{EB}(n+1) - H_{EB}(n) = \gamma(H_{EB}(n) - H_{E\infty})^3, \quad (3)$$

where γ = sample dependent constant (= $1/2k^2$) and $H_{E\infty}$ = exchange bias field in $n \to \infty$. Using $\gamma = 1.28\times10^{-6}$ Oe^{-2} and $H_{E\infty}$ = 606.24 Oe (generated from the power law fitting as shown in Equation (2)) as an additional input in Equation (3), the whole set of results can be generated for H_{EB}. We displayed the obtained results by open (orange) triangles in Figure 9b. We list all magnetic parameters in Table 2.

Table 2. Magnetic parameters for Ba_2ScRuO_6.

Parameters	Unit	Ba_2ScRuO_6
Crystallite size (D)	nm	46 nm
Transition temperature (T_N)	K	9
Weiss temperature	K	−694
Frustration parameter (f)	-	77
Cooling field (H_{FC})	kOe	20 kOe
Exchange bias field (H_{EB})	kOe	1.24 (at 2 K)
Exchange bias field $n \to \infty$ ($H_{E\infty}$)	Oe	606.24

Giant EB effects have recently been reported in several similar double perovskite materials having cationic disorders (for instance, in hexagonal $Ba_2Fe_{1.12}Os_{0.88}O_6$ [39], in Gd_2CoRuO_6 [30], and in $LaSrCoFeO_6$ [31]). The presence of antisite disorder originates from competing magnetic interactions and frustrations in the system and is attributed to the huge EB effects in these systems. Material systems with different crystallographic sites for magnetic cations are prone to antisite disorder. In the present material, a disorder between Ru-Sc is observed at both the Sc2 (M3, 1a, corner-sharing B_2O_6 sites) and Ru2 (M4, 2d, face-sharing B_2O_9 dimer) sites. However, the degree of disorder is less than the $Ba_2Fe_{1.12}Os_{0.88}O_6$ material. Therefore, similar to the $Ba_2Fe_{1.12}Os_{0.88}O_6$ and other related materials, the disorder in Sc-Ru, which is creating magnetic frustration, is responsible for the EB effect in Ba_2ScRuO_6 below the AFM ordering temperature.

4. Conclusions

In conclusion, the ambient pressure synthesized Ba_2ScRuO_6 is found to crystallize in a 6L hexagonal structure (space group $P\bar{3}m1$) at room temperature. Electron conduction corresponds to the Mott 3D-VRH model, and the disorder initiates carrier localization. This antiferromagnetic double perovskite compound Ba_2ScRuO_6 shows an exchange bias below the long-range antiferromagnetic ordering (T_N = 9 K). The exchange bias effect is seen below the AFM ordering temperature when the sample is cooled in the presence of a magnetic field (H_{FC} = 20 kOe) and reaches a maximum value of 1.24 kOe at 2 K. Furthermore, exchange bias is supported by training effect studies. Inhomogeneous magnetic correlations and magnetic frustration formed due to the disorder of magnetic (Ru) and nonmagnetic (Sc) cations at both the Sc2 (1a, corner-sharing B_2O_6 sites) and Ru2 (2d, face-sharing B_2O_9 dimer) sites. The magnetic frustrations in the structure below the long-range AFM ordering create a large EB effect in this sample. This indicates that cationic disorder-induced magnetic frustration can be used to trigger the exchange bias effect. Furthermore, our study suggests that the frustrated hexagonal double perovskite systems are a promising family of compounds to explore new materials that have a large exchange bias effect.

Author Contributions: Formal analysis, P.M. and S.M.; Investigation, P.M. and S.M.; Writing—original draft, S.M. and R.P.S.; Writing—review & editing, S.M. and R.P.S.; Supervision, R.P.S. All authors have read and agreed to the published version of the manuscript.

Funding: R.P.S. acknowledges the Science and Engineering Research Board (SERB), Government of India, for the CRG/2019/001028 Core Research Grant. S.M. acknowledges the Science and Engineering Research Board, Government of India for the SRG/2021/001993 Start-up Research Grant.

Institutional Review Board Statement: Not applicable.

Informed Consent Statement: Not applicable.

Data Availability Statement: Data will be made available on request.

Conflicts of Interest: The authors declare no conflict of interest.

References

1. Kobayashi, K.I.; Kimura, T.; Sawada, H.; Terakura, K.; Tokura, Y. Room-temperature magnetoresistance in an oxide material with an ordered double-perovskite structure. *Nature* **1998**, *395*, 677. [CrossRef]
2. Serrate, D.; Teresa, J.M.D.; Ibarra, M.R. Double perovskites with ferromagnetism above room temperature. *J. Phys. Condens. Matter* **2007**, *19*, 023201. [CrossRef]
3. Kato, H.; Okuda, T.; Okimoto, Y.; Tomioka, Y.; Takenoya, Y.; Ohkubo, A.; Kawasaki, M.; Tokura, Y. Metallic ordered double-perovskite Sr_2CrReO_6 with maximal Curie temperature of 635 K. *Appl. Phys. Lett.* **2002**, *81*, 328. [CrossRef]
4. Das, H.; Sanyal, P.; Saha-Dasgupta, T.; Sharma, D.D. Origin of magnetism and trend in T_c in Cr-based double perovskites: Interplay of two driving mechanisms. *Phys. Rev. B* **2011**, *83*, 104418. [CrossRef]
5. Narayanan, N.; Mikhailova, D.; Senyshyn, A.; Trots, D.M.; Laskowski, R.; Blaha, P.; Schwarz, K.; Fuess, H.; Ehrenberg, H. Temperature and composition dependence of crystal structures and magnetic and electronic properties of the double perovskites $La_{2-x}Sr_xCoIrO_6$ ($0 \leq x \leq 2$). *Phys. Rev. B* **2010**, *82*, 024403. [CrossRef]
6. Kolchinskaya, A.; Komissinskiy, P.; Baghaie, Y.M.; Vafaee, M.; Mikhailova, D.; Narayanan, N.; Ehrenberg, H.; Wilhelm, F.; Rogalev, A.; Alff, L. Magnetism and spin-orbit coupling in Ir-based double perovskites $La_{2-x}Sr_xCoIrO_6$. *Phys. Rev. B* **2012**, *85*, 224422. [CrossRef]
7. Feng, H.L.; Schnelle, W.; Tjeng, L.H.; Jansen, M. Synthesis, crystal structures, and magnetic properties of double perovskites $SrLaNiOsO_6$ and $BaLaNiOsO_6$. *Solid State Commun.* **2016**, *243*, 49. [CrossRef]
8. Morrow, R.; Yan, J.; McGuire, M.A.; Freeland, J.W.; Haskel, D.; Woodward, P.M. Effects of chemical pressure on the magnetic ground states of the osmate double perovskites $SrCaCoOsO_6$ and Ca_2CoOsO_6. *Phys. Rev. B* **2015**, *92*, 094435. [CrossRef]
9. Wang, H.; Zhu, S.; Ou, X.; Wu, H. Ferrimagnetism in the double perovskite Ca_2FeOsO_6: A density functional study. *Phys. Rev. B* **2014**, *90*, 054406. [CrossRef]
10. Hou, Y.S.; Xiang, H.J.; Gong, X.G. Lattice-distortion Induced Magnetic Transition from Low-temperature Antiferromagnetism to High-temperature Ferrimagnetism in Double Perovskites A_2FeOsO_6 (A= Ca, Sr). *Sci. Rep.* **2015**, *5*, 13159. [CrossRef]
11. Nilsen, G.J.; Thompson, C.M.; Ehlers, G.; Marjerrison, C.A.; Greedan, J.E. Diffuse magnetic neutron scattering in the highly frustrated double perovskite Ba_2YRuO_6. *Phys. Rev. B* **2015**, *91*, 054415. [CrossRef]
12. Carlo, J.P.; Clancy, J.P.; Fritsch, K.; Marjerrison, C.A.; Granroth, G.E.; Greedan, J.E.; Dabkowska, H.A.; Gaulin, B.D. Spin gap and the nature of the $4d^3$ magnetic ground state in the frustrated fcc antiferromagnet Ba_2YRuO_6. *Phys. Rev. B* **2013**, *88*, 024418. [CrossRef]
13. Dass, R.I.; Yan, J.Q.; Goodenough, J.B. Ruthenium double perovskites: Transport and magnetic properties. *Phys. Rev. B* **2004**, *69*, 094416. [CrossRef]
14. Hinatsu, Y.; Izumiyama, Y.; Doi, Y.; Alemi, A.; Wakeshima, M.; Nakamura, A.; Morii, Y.J. Studies on magnetic and calorimetric properties of double perovskites Ba_2HoRuO_6 and Ba_2HoIrO_6. *Solid State Chem.* **2004**, *177*, 38. [CrossRef]
15. Hong, K.P.; Choi, Y.H.; Kwon, Y.U.; Jung, D.Y.; Lee, J.S.; Shim, H.S.; Lee, C.H. Atomic and magnetic long-range orderings in $BaLaMRuO_6$ (M= Mg and Zn). *J. Solid State Chem.* **2000**, *150*, 383. [CrossRef]
16. Battle, P.D.; Goodenough, J.B.; Price, R.J. The crystal structures and magnetic properties of Ba_2LaRuO_6 and Ca_2LaRuO_6. *Solid State Chem.* **1983**, *46*, 234. [CrossRef]
17. Battle, P.D.; Jones, C.W.J. The crystal and magnetic structures of Sr_2LuRuO_6, Ba_2YRuO_6, and Ba_2LuRuO_6. *Solid State Chem.* **1989**, *78*, 108. [CrossRef]
18. Battle, P.D.; Macklin, W.J. The crystal and magnetic structures of Sr_2YRuO_6. *J. Solid State Chem.* **1984**, *52*, 138. [CrossRef]
19. Disseler, S.M.; Lynn, J.W.; Jardim, R.F.; Torikachvili, M.S.; Granado, E. Spin dynamics and two-dimensional correlations in the fcc antiferromagnetic Sr_2YRuO_6. *Phys. Rev. B* **2016**, *93*, 140407. [CrossRef]
20. Aczel, A.A.; Baker, P.J.; Bugaris, D.E.; Yeon, J.; Loye, H.C.Z.; Guidi, T.; Adroja, D.T. Exotic Magnetism on the Quasi-fcc Lattices of the d^3 Double Perovskites $La_2NaB'O_6$ (B'= Ru, Os). *Phys. Rev. Lett.* **2014**, *112*, 117603. [CrossRef]
21. Ranjbar, B.; Pavan, A.; Kennedy, B.J.; Zhang, Z.M. Structural and magnetic properties of the ruthenium double perovskites $Ba_{2-x}Sr_xYRuO_6$. *Dalton Trans.* **2015**, *44*, 10689. [CrossRef]
22. Granado, E.; Lynn, J.W.; Jardim, R.F.; Torikachvili, M.S. Two-Dimensional Magnetic Correlations and Partial Long-Range Order in Geometrically Frustrated Sr_2YRuO_6. *Phys. Rev. Lett.* **2013**, *110*, 017202. [CrossRef] [PubMed]
23. Takahashi, R.; Okazaki, R.; Yasui, Y.; Terasaki, I.; Sudayama, T.; Nakao, H.; Yamasaki, Y.; Okamoto, J.; Murakami, Y.; Kitajima, Y.J. High-temperature thermoelectric properties of the double-perovskite ruthenium oxide $(Sr_{1-x}La_x)_2ErRuO_6$. *Appl. Phys.* **2012**, *112*, 073714. [CrossRef]

24. Cetin, S.K.; Akca, G.; Kaya, D.; Ayas, A.O.; Ekicibil, A. Synthesis and characterization of bifunctional Ru doped La-based perovskites for magnetic refrigeration and energy storage systems. *Int. J. Hydrogen Energy* **2022**, *47*, 40999. [CrossRef]
25. Dani, S.; Arya, A.; Sharma, H.; Kumar, R.; Goyal, N.; Kumar, R.; Pandit, R. Structural and electronic properties of double perovskite ruthenates; A_2GdRuO_6 (where A= Ba, Sr). *J. Alloys Compd.* **2022**, *913*, 165177. [CrossRef]
26. Guenez, W.; Bouguerra, A.; Touaibia, I.; Chemam, F. Giant magneto optical properties in the double perovskites $Ba_2B'RuO_6$ (B'= Er, Tm). *J. Phys. Condens. Matter* **2022**, *34*, 505501. [CrossRef]
27. Singh, R.P.; Tomy, C.V. Anomalous magnetic properties of Sr_2YRuO_6. *Phys. Rev. B* **2008**, *78*, 024432. [CrossRef]
28. Aharen, T.; Greedan, J.E.; Ning, F.L.; Imai, T.; Michaelis, V.K.; Kroeker, S.; Zhou, H.D.; Wiebe, C.R.; Cranswick, L.M.D. Magnetic properties of the S= 3/2 geometrically frustrated double perovskites La_2LiRuO_6 and Ba_2YRuO_6. *Phys. Rev. B* **2009**, *80*, 134423. [CrossRef]
29. Aczel, A.A.; Bugaris, D.E.; Li, L.; Yan, J.-Q.; Cruz, C.d.; Loye, H.-C.z.; Nagler, S.E. Frustration by competing interactions in the highly distorted double perovskites $La_2NaB'O_6$ (B'= Ru, Os). *Phys. Rev. B* **2013**, *87*, 014435. [CrossRef]
30. Das, M.; Dutta, P.; Giri, S.; Majumdar, S.; Bandyopadhyay, A.; Yadav, A.K.; Jha, S.N.; Bhattacharyya, D.; Das, G.; Rajaji, V. Cationic disorder: A pathway for demonstrating inverse exchange bias in Gd_2CoRuO_6. *Phys. Rev. B* **2020**, *101*, 064419. [CrossRef]
31. Sahoo, R.C.; Takeuchi, Y.; Ohtomo, A.; Hossain, Z. Exchange bias and spin glass states driven by antisite disorder in the double perovskite compound $LaSrCoFeO_6$. *Phys. Rev. B* **2019**, *100*, 214436. [CrossRef]
32. Hissariya, R.; Sathe, V.G.; Mishra, S.K. Antisite disorder mediated exchange bias effect and spin-glass state in $La_{2-x}Sm_xNiMnO_6$. *J. Magn.Magn. Mater.* **2023**, *578*, 170769. [CrossRef]
33. Kayser, P.; Injac, S.; Ranjbar, B.; Kennedy, B.J. Magnetic and Structural Studies of Sc Containing Ruthenate Double Perovskites A_2ScRuO_6 (A = Ba, Sr). *Inorg. Chem.* **2017**, *56*, 9009. [CrossRef] [PubMed]
34. Shannon, R. Revised effective ionic radii and systematic studies of interatomic distances in halides and chalcogenides. *Acta Crystallogr. Sect. A* **1976**, *32*, 751. [CrossRef]
35. Mott, N.F. Conduction in non-crystalline materials: III. Localized states in a pseudogap and near extremities of conduction and valence bands. *Philos. Mag.* **1969**, *19*, 835. [CrossRef]
36. Morrow, R.; Samanta, K.; Dasgupta, T.S.; Xiong, J.; Freeland, J.W.; Haskel, D.; Woodward, P.M. Magnetism in Ca_2CoOsO_6 and Ca_2NiOsO_6: Unraveling the Mystery of Superexchange Interactions between 3d and 5d Ions. *Chem. Mater.* **2016**, *28*, 3666. [CrossRef]
37. Senn, M.S.; Kimber, S.A.J.; Lopez, A.M.A.; Hill, A.H.; Attfield, J.P. Spin orders and lattice distortions of geometrically frustrated 6H-perovskites $Ba_3B'Ru_2O_9$ (B'= La^{3+}, Nd^{3+}, and Y^{3+}). *Phys. Rev. B* **2013**, *87*, 134402. [CrossRef]
38. Paul, A.K.; Jansen, M.; Yan, B.; Felser, C.; Reehuis, M.; Abdala, P.M. Synthesis, Crystal Structure, and Physical Properties of Sr_2FeOsO_6. *Inorg. Chem.* **2013**, *52*, 6713. [CrossRef]
39. Feng, H.L.; Adler, P.; Reehuis, M.; Schnelle, W.; Pattison, P.; Hoser, A.; Felser, C.; Jansen, M. High-Temperature Ferrimagnetism with Large Coercivity and Exchange Bias in the Partially Ordered 3d/5d Hexagonal Perovskite $Ba_2Fe_{1.12}Os_{0.88}O_6$. *Chem. Mater.* **2017**, *29*, 886. [CrossRef]
40. Mohanty, P.; Marik, S.; Singh, D.; Singh, R.P. Room temperature magnetoresistance and exchange bias in "314-type" oxygen-vacancy ordered $SrCo_{0.85}Fe_{0.15}O_{2.62}$. *Appl. Phys. Lett.* **2017**, *111*, 022402. [CrossRef]
41. Marik, S.; Mohanty, P.; Singh, D.; Singh, R.P. Moderate magnetic field induced large exchange bias effect in ferrimagnetic 314—$Sr_3YCo_4O_{10.5}$ material. *J. Phys. D Appl. Phys.* **2018**, *51*, 065006. [CrossRef]
42. Tsang, C.; Fontana, R.E.; Lin, T.; Heim, D.; Speriosu, V.S.; Gurney, B.A.; Williams, M.L. Design, fabrication and testing of spin-valve read heads for high density recording. *IEEE Trans. Magn.* **1994**, *30*, 3801. [CrossRef]
43. Prejbeanu, I.L.; Kerekes, M.; Sousa, R.C.; Sibuet, H.; Redon, O.; Dieny, B.; Nozieres, J.P. Thermally assisted MRAM. *J. Phys. Condens. Matter* **2007**, *19*, 165218. [CrossRef]
44. Chen, Y.T.; Jen, S.U.; Yao, Y.D.; Wu, J.M.; Liao, J.H.; Wu, T.B. Exchange biasing observed in the $Co/Ir_{20}Mn_{80}$ system. *J. Alloys Compd.* **2008**, *448*, 59. [CrossRef]
45. Fuke, H.; Kamiguchi, Y.; Hashimoto, S.; Funiyama, T.; Saito, K.; Iwasaki, H.; Sahashi, M. Exchange coupling film and magnetoresistive element. U.S. Patent 6057049, 2 May 2000.
46. Singh, R.P.; Tomy, C.V.; Grover, A.K. Observation of tunable exchange bias in Sr_2YbRuO_6. *Appl. Phys. Lett.* **2010**, *97*, 182505. [CrossRef]
47. Kurian, M.M.; Das, R.R.; Devan, C.V.; Varma, M.R.; Colin, C.V.; Santhosh, P.N. Exchange bias effect and inhomogeneous magnetism in 6H $Ba_3CoFeRuO_9$: Role of structural site disorder. *J. Magn. Magn. Mater.* **2023**, *568*, 170372. [CrossRef]
48. Hoffmann, A. Symmetry driven irreversibilities at ferromagnetic-antiferromagnetic interfaces. *Phys. Rev. Lett.* **2004**, *93*, 097203. [CrossRef]
49. Binek, C.; Polisetty, S.; He, X.; Berger, A. Exchange bias training effect in coupled all ferromagnetic bilayer structures. *Phys. Rev. Lett.* **2006**, *96*, 067201. [CrossRef]
50. Binek, C. Training of the exchange-bias effect: A simple analytic approach. *Phys. Rev. B* **2004**, *70*, 014421. [CrossRef]